

Stress variation analysis based on temperature measurements at Zhuhai Opera House

Wei Lu, Jun Teng*, Lihang Qiu and Kai Huang

Harbin Institute of Technology (Shenzhen), China

(Received November 12, 2017, Revised February 16, 2018, Accepted February 24, 2018)

Abstract. The Zhuhai Opera House has an external structure consisting of a type of spatial steel, where the stress of steel elements varies with the ambient temperature. A structural health monitoring system was implemented at Zhuhai Opera House, and the temperatures and stresses of the structures were monitored in real time. The relationship between the stress distribution and temperature variations was analysed by measuring the temperature and stresses of the steel elements. In addition to measurements of the structure stresses and temperatures, further simulation analysis was carried out to provide the detailed relationship between the stress distributions and temperature variations. The limited temperature measurements were used to simulate the structure temperature distribution, and the stress distributions of all steel elements of the structure were analysed by building a finite element model of the Zhuhai Opera House spatial steel structure. This study aims to reveal the stress distributions of steel elements in a real-world project based on temperature variations, and to supply a basic database for the optimal construction time of a spatial steel structure. This will not only provide convenient, rapid and safe early warnings and decision-making for the spatial steel structure construction and operation processes, but also improve the structural safety and construction accuracy of steel space structures.

Keywords: structural health monitoring; stress variation; temperature measurements; Zhuhai Opera House

1. Introduction

Structural health monitoring is being applied increasingly in spatial steel structures (Teng *et al.* 2015, Teng *et al.* 2012). The use of existing monitoring data to realize the structure of the identified stress field distribution is significant in practical engineering (Yi *et al.* 2017, Mao *et al.* 2018). A structure is mainly influenced by temperatures and wind loads during operation. Certain scholars have conducted research on the non-uniform distribution of thermal effects (Pei *et al.* 2008, Real *et al.* 2007). Research on spatial steel structure temperature effects mainly refers to studying structural strain and stress under the temperature effect. A spatial steel structure, which is a type of high-order statically indeterminate structure with a temperature response that is positively correlated to the thermal expansion coefficient of structural materials, statically indeterminate number of structures and non-uniformity of the temperature field distribution. Spatial steel structures are generally exposed directly to the sun, and steel structure deformation, which is

*Corresponding author, Professor, E-mail: tengj@hit.edu.cn

caused by temperature changes, includes axial, bending and surface deformations. Under additional constraints, these deformations will result in a temperature sub-internal force. As the structure span and bar length increase, the deformation caused by repeated changes in temperature will accumulate continuously, resulting in fatigue damage to the structural member (Lin and Stotesbury 1981). Therefore, studying the temperature effect is of great significance for the design and safe use of spatial steel structures. Monitoring variables for structural health monitoring mainly include temperature, displacement, strain and stress (Bueno and Sales 2010, Jiang and Hua 2013, Ni *et al.* 2011, Zhou and Hua 2008). Numerous studies have demonstrated the effectiveness of structural health monitoring in surveillance (Cao *et al.* 2011), including frequency response (Halling and Barr 2006, Mooney 2005, Friswell and Imregun 2007), the monitoring method (Taha and Ross 2007), statistical processing (Czarnecki and Farrar 2000), displacement analysis and strain analysis (Cardini and Dewolf 2008, Howell and Shenton 2006, Watson and Coleman 2007).

In this paper, based on the non-uniform environmental loads, stress variation analysis of spatial steel structures using temperature measurements is proposed. First, the structural health monitoring system for the small shell structure of the Zhuhai Opera House is introduced, including the locations of temperature monitoring points. Second, the temperature distribution of the structure is proposed, based on the structural temperature partition methods and temperature measurements. By combining the small shell structure of the Zhuhai Opera House, the entire process is illustrated and the stress variation analysis is provided, from which the stress statuses caused by temperature variations are offered.

2. SHM system of the small shell structure

For the small theatre, Zhuhai Opera House, the main body ground and underground height are 18 m and 4.5 m, respectively, while the shell height is 55.6 m. The temperature difference in Zhuhai is significant, as the lowest temperature is approximately 5°C to 10°C, while the maximum may reach 34°C to 36°C. Therefore, the influence of the thermal effect on the Zhuhai Opera House should be considered. The small shell structure monitoring system includes the stress and temperature monitoring. The locations for the stress and temperature monitoring are the same; that is, 12 monitoring points were selected for installing the strain and temperature sensors, with two sensors at one monitoring point.

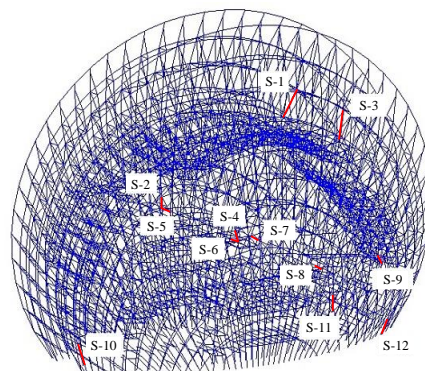


Fig. 1 Monitoring points distribution

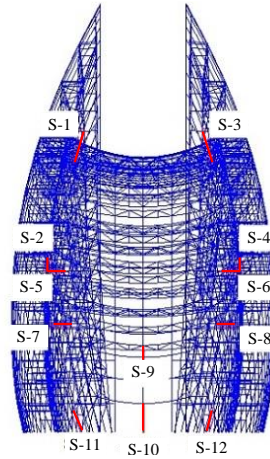


Fig. 2 Side view of point distribution

The monitoring frequency is two times a day, and the specific measuring time is 8 to 9 o'clock in the morning and 4 to 5 o'clock in the afternoon. The measuring points on the shell structure are illustrated in Figs. 1 and 2. The numbering rule of the monitoring point is “S-n”, where S means the small theatre of Zhuhai Opera House, n is the serial number of measuring point.

3. Structural temperature partition method

3.1 Solar radiation cumulant

The meshed model was imported into the Ecotect Analysis 2011, as shown in Fig. 3. The time points of the sunrise/sunset in Zhuhai for the entire year were counted and set up for the analysis of incident solar radiation, as indicated in Fig. 4. Furthermore, the solar radiation cumulant W of years 2014 and 2015 were calculated. Because the Ecotect Analysis can only calculate the period for which the time points of the sunrise/sunset are nearly the same, while the time points of the sunrise/sunset in the three months of each quarter differ, the average value of time points of the sunrise/sunset were selected to calculate the solar radiation cumulant, as illustrated in Fig. 5.

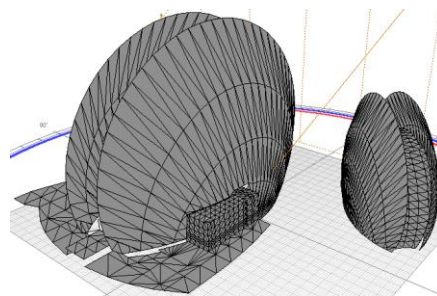


Fig. 3 Ecotect Analysis model

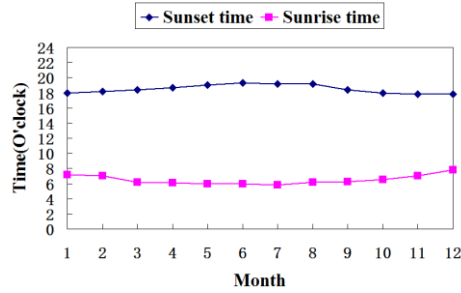
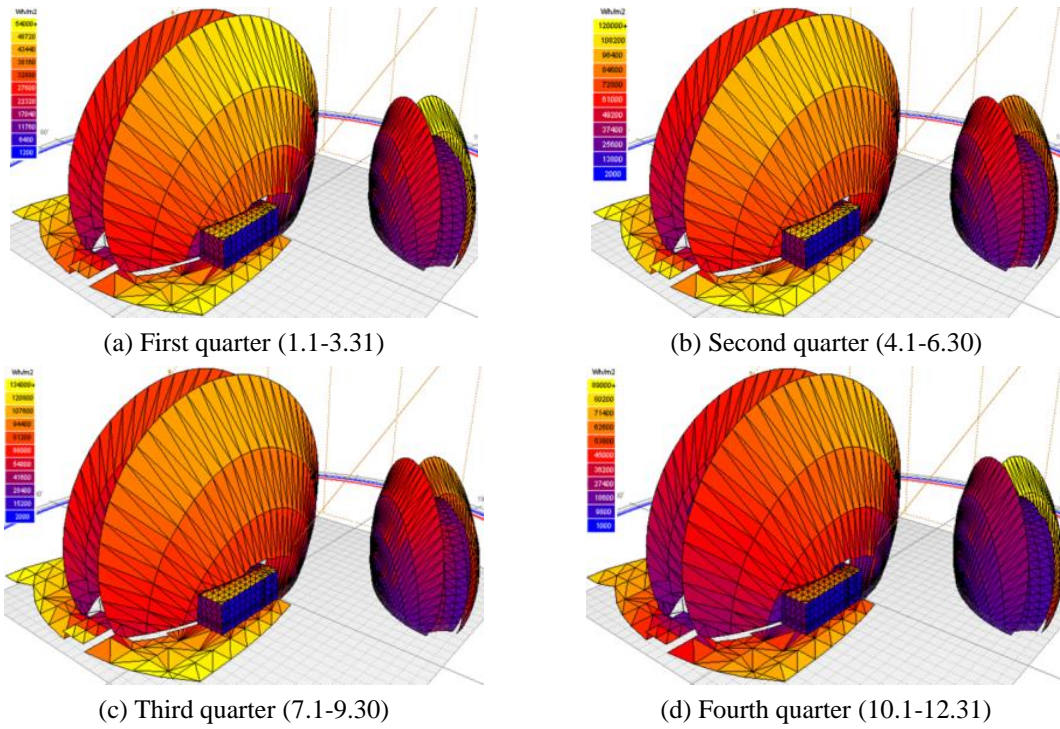


Fig. 4 Entire year's sunrise and sunset time in Zhuhai

Fig. 5 Distribution conditions of solar radiation cumulant W in each quarter

3.2 Structural temperature partitions based on solar radiation cumulant value

According to the numerical variation in the solar radiation cumulant on the small shell surface, the areas with numerical similarity in the cumulant value were classified as the same partition. There were four partitions in total. Sorting the solar radiation cumulant values from high to low yields $W_I > W_{II} > W_{III} > W_{IV}$, as shown in Fig. 6.

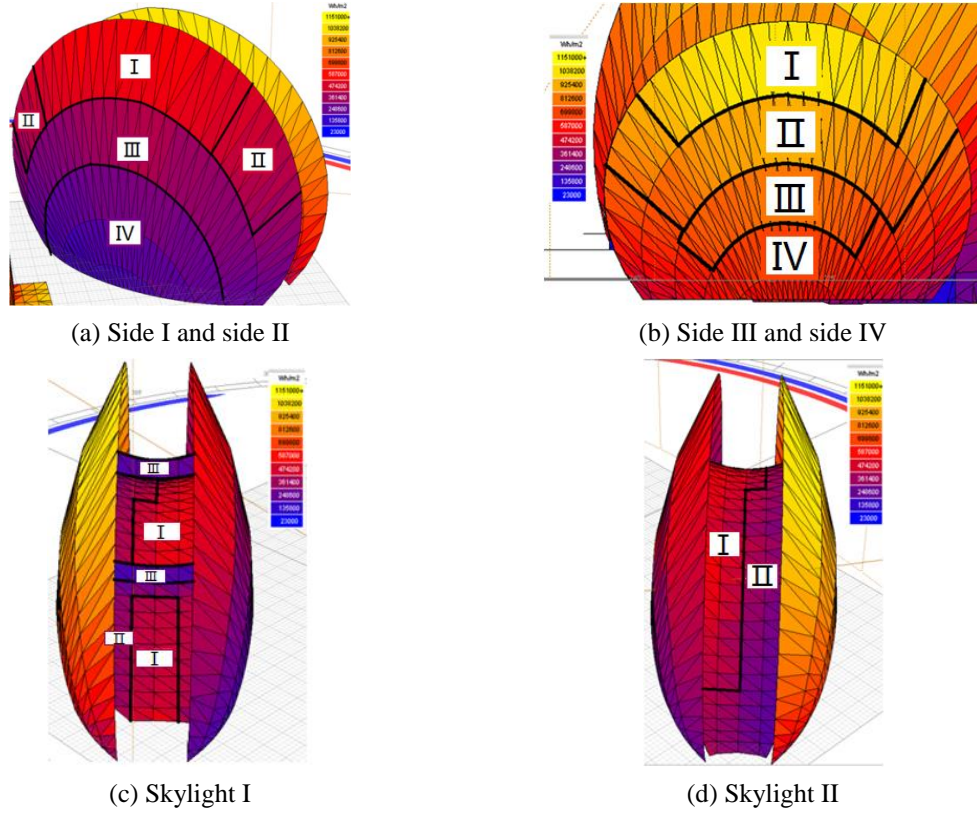


Fig. 6 Temperature partitions of small shell

3.3 Standard and reference regions

Partition III, which had the greatest number of sensors installed within the four partitions, was selected as the standard region p . The reference region q was partition IV, as it was the runner-up in terms of sensor numbers. The average values of the two partition temperatures were T_{III}^M and T_{IV}^M , respectively. These were selected as the representative values for the standard region.

4. Calculation method for temperature values in temperature partitions

4.1 Temperature variation ratio

The calculation formula for the temperature variation based on the solar radiation cumulant value is expressed as

$$\Delta T = \frac{\Delta W}{cm} \quad (1)$$

where c denotes the specific heat capacity, m is the mass, ΔW is the variation value of the solar

radiation cumulant, and ΔT is the temperature variation value. According to the above formula, if there were no outside interference, ΔT and ΔW would have a linear relationship when c and m were unchanged. For the structures, if the environmental influence on the temperature fields is not considered, in theory, the temperature variation value on the structure surfaces and variation of solar radiation cumulant would have a linear relationship. Therefore, the temperature variation ratio α_{iq} can be identified as Eq. (2)

$$\alpha_{iq} = \frac{W_i - W_q}{W_p - W_q} = \frac{T_i - T_q}{T_p - T_q} \quad (2)$$

where W_i , W_p and W_q denote the solar radiation cumulant values of partitions i , p and q , respectively, while T_i , T_p and T_q are the temperature values of partitions i , p and q , respectively.

The solar radiation cumulant values and temperature variation ratio of each partition can be seen in Table 1.

4.2 Partition temperature representative values

In order to calculate the partition temperature representative values T_i^S , in addition to the standard region p and reference region q , the simulative representative values of the other partitions i were required, as shown in Eq. (3)

$$T_i^S = \alpha_{iq}(T_p^M - T_q^M) + T_q^M \quad (3)$$

where α_{iq} is the temperature variation ratio; T_p^M is the average value of the measured temperature of the standard region p ; T_q^M is the average value of the measured temperature of the reference region q .

Only two monitoring points were arranged on the skylight parts. Therefore, the actual monitoring temperature values were selected to determine the partition temperature representative values, as the sensors were limited in number. That is, besides the standard region III and reference region IV, the simulative representative values of the other partitions were calculated using Eq. (3).

Table 1 Sensor distribution conditions of each partition

Positions	Partitions	Sensor serial numbers	W_i (Wh/m ²)	Proportion α_{iq}
Sides 1 and 2	I	S-1	49000	2.33
Sides 1 and 2	II	--	39400	1.67
Sides 1 and 2	III	S-2 S-5 S-7	29800	1.00
Sides 1 and 2	IV	S-11	15400	0.00
Sides 3 and 4	I	S-3	97000	2.18
Sides 3 and 4	II	--	87400	1.59
Sides 3 and 4	III	S-4 S-6 S-8	77800	1.00
Sides 3 and 4	IV	S-12	61480	0.00

Table 2 Actual monitoring temperature and simulative representative temperature of three days

Positions	Partitions	Dates					
		May 19 th afternoon		July 30 th morning		October 7 th morning	
		AMT (°C)	SRT (°C)	AMT (°C)	SRT (°C)	AMT (°C)	SRT (°C)
Sides 1 and 2	I	29.35	29.58	29.65	29.51	29	27.76
Sides 1 and 2	II	29.42	29.53	29.3	29.26	27.85	27.23
Sides 1 and 2	III	29.48	29.48	29.01	29.02	26.7	26.7
Sides 1 and 2	IV	29.4	29.4	28.6	28.6	25.8	25.8
Sides 3 and 4	I	29.75	29.56	29.1	31.59	25	28.23
Sides 3 and 4	II	29.63	29.53	29.44	30.69	25.98	27.6
Sides 3 and 4	III	29.5	29.5	29.78	29.78	26.97	26.97
Sides 3 and 4	IV	29.45	29.45	28.25	28.25	25.9	25.9
Skylight	I	29.3	29.3	28.7	28.7	25.8	25.8
Skylight	II	29.8	29.8	29.15	29.15	27.85	27.85
Skylight	III	29.55	29.55	28.93	28.93	26.83	26.83

*AMT = Actual Monitoring Temperature; SRT = Simulative Representative Temperature

The actual monitoring temperature values of May 19th afternoon, July 30th morning and October 7th morning in 2014 were selected for calculating the partition temperature representative values, as shown in Table 2.

5. Stress distribution caused by temperature effect

In order to investigate the relationship between the overall temperature difference and response, members that had tensile and pressure stresses in the top 100 were selected, with $\Delta T = +6^\circ\text{C}$. The different T_σ ranges were selected to calculate the temperature values for different dates, and the member stress distributions are shown in Table 3. As the variations in member stress positions under different ranges were very small, members with tensile and pressure stresses in the top 100 were selected as research objects to observe these variations more conveniently. Therefore, according to the stress distribution results, the member distribution on the morning of May 4th ($T_\sigma = 0.11^\circ\text{C}$) was close to that in the afternoon of February 23rd ($T_\sigma = 0.99^\circ\text{C}$), while the member distribution on the morning of April 5th ($T_\sigma = 2.75^\circ\text{C}$) was close to that in the afternoon of January 18th ($T_\sigma = 2.09^\circ\text{C}$).

Table 3 Temperature measurements for each period

	May 4 th morning	February 23 rd afternoon	April 5 th afternoon	January 18 th afternoon
Mean square error of temperature T_σ (°C)	0.11	0.99	2.75	2.09
Overall temperature T (°C)	22.56	19.14	24.77	21.37
Initial temperature T_0 (°C)	18.97	18.97	18.97	18.97
Temperature difference ΔT (°C)	3.59	0.17	5.80	2.40

6. Longitudinal response characteristics at different times within a year

6.1 Selection of key points of load effect

The key time describing the overall temperature change throughout the year is selected as the key point, and the temperature field is simulated based on the measured temperature data of the key points. To study the response distribution, the temperature effects and self-weight are applied together in the finite element model, so that the responses at different key times can be obtained.

The temperature data for 2014 was selected as the research object because of the data integrity. The selection of key points must consider two influencing factor types in the temperature field: the overall temperature difference value and the mean square error of the temperature value. The overall temperature difference value lies within the scope of $[-12, 12]$ and two different situations exist for each key point, namely $0 \leq T_{\sigma} \leq 2$ and $2 \leq T_{\sigma} \leq 5$.

According to the above conditions, we can select the key points from the 2014 temperature data and determine the regional temperature representative value to obtain the calculated response. The key point temperature information for both cases can be seen in Tables 4 and 5.

6.2 Calculation results and conclusion analysis

As the temperature changes, the structural member response will always be under pressure, intension, or fluctuating between tension and pressure. If the bar responses change within a wide range, their performance will change or suffer fatigue damage, which will lead to local structural defects and even affect the overall structural safety.

Table 4 Key point temperature information for $0 \leq T_{\sigma} \leq 2$

	February 13 th morning	February 22 th morning	April 21 th morning	August 11 th afternoon	October 13 th morning
Overall temperature T (°C)	6.50	12.93	24.33	30.56	25.30
Mean square error T_{σ} (°C)	0.47	0.57	0.15	0.67	0.93
Initial temperature T_0 (°C)	18.97	18.97	18.97	18.97	18.97
Temperature difference ΔT (°C)	-12.47	-6.04	5.36	11.59	6.33

Table 5 Key point temperature information for $2 \leq T_{\sigma} \leq 5$

	January 12 th afternoon	January 22 th morning	April 5 th afternoon	June 4 th afternoon	April 9 th afternoon
Overall temperature T (°C)	7.98	12.88	24.92	30.93	25.10
Mean square error T_{σ} (°C)	2.20	2.48	2.35	2.5	2.05
Initial temperature T_0 (°C)	18.97	18.97	18.97	18.97	18.97
Temperature difference ΔT (°C)	-10.99	-6.09	5.92	11.96	6.13

Therefore, to further understand this structural behaviour, based on the above 10 sets of conditions for structure response information, we categorise three cases, namely always under pressure, always in tension and fluctuating between tension and pressure, to describe the bar response characteristics under 10 condition sets. The formulae for the response change amplitude of bar i are

$$\text{Always in tension} \quad \Delta\sigma_i = \sigma_{\max,i}^T - \sigma_{\min,i}^T \quad (4)$$

$$\text{Always under pressure} \quad \Delta\sigma_i = \sigma_{\max,i}^P - \sigma_{\min,i}^P \quad (5)$$

$$\text{Fluctuating between tension and pressure} \quad \Delta\sigma_i = \sigma_{\max,i}^T - \sigma_{\min,i}^P \quad (6)$$

where $\Delta\sigma_i$ represents the response change amplitude of bar i in 10 condition sets, $\Delta\sigma_{\max,i}^T$ is the response maximum tensile stress of bar i , $\Delta\sigma_{\min,i}^T$ is the response minimum tensile stress of bar i , $\Delta\sigma_{\max,i}^P$ is the response maximum pressure stress of bar i , and $\Delta\sigma_{\min,i}^P$ is the response minimum pressure stress of bar i .

To ensure the bar response for the above conditions is described fully, in the process of researching the amplitude of the bar response changes, the absolute value of the bar response should also be explored. In order to compare the three changes σ_{\max} , σ_{\min} and $\Delta\sigma$ more conveniently, the response change amplitudes $\Delta\sigma$ of bars were arranged in descending order, and the first 300 bars were selected to compare the changes of σ_{\max} and σ_{\min} . This displays the response information of bars always in tension, always under pressure and fluctuating between tension and pressure within a year.

(1) Response information of bars that are always under pressure. The overall distribution of 10 sets of bars that were always under pressure can be seen in Fig. 7. The changes in σ_{\max}^P and σ_{\min}^P are compared with the descending sorting of $\Delta\sigma$, as shown in Fig. 8.

(2) Response information of bars that are always in tension. The overall distribution of 10 sets of bars that were always in tension can be seen in Fig. 9. The changes in σ_{\max}^T and σ_{\min}^T are compared with the descending sorting of $\Delta\sigma$, as shown in Fig. 10.

(3) Response information of bars that fluctuate between tension and pressure. The overall distribution of 10 sets of bars that fluctuated between tension and pressure can be seen in Fig. 11. The changes in σ_{\max}^T and σ_{\min}^P are compared with the descending sorting of $\Delta\sigma$, as shown in Fig. 12.

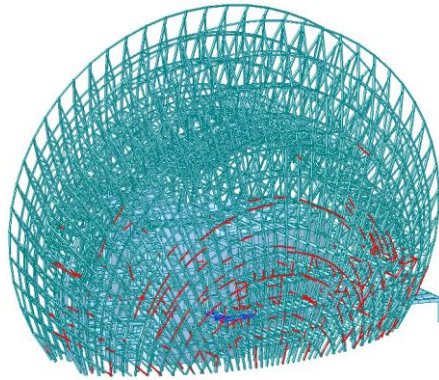


Fig. 7 Overall distribution of 10 sets of bars always under pressure

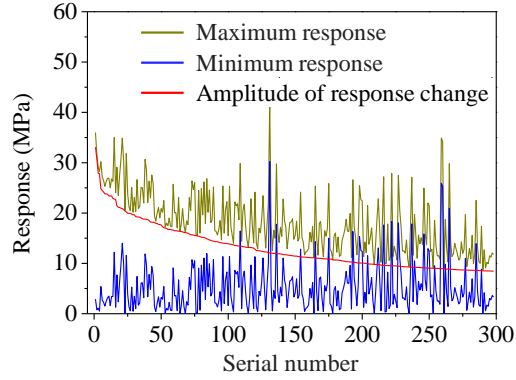


Fig. 8 Changes in σ_{\max}^p and σ_{\min}^p with descending sorting of $\Delta\sigma$

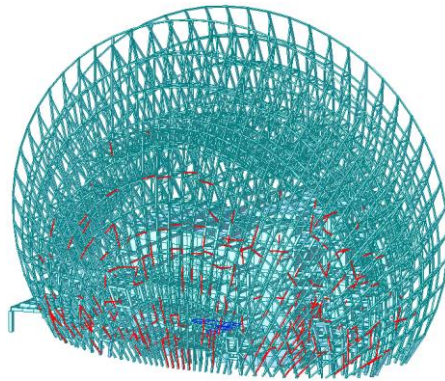


Fig. 9 Overall distribution of 10 sets of bars always in tension

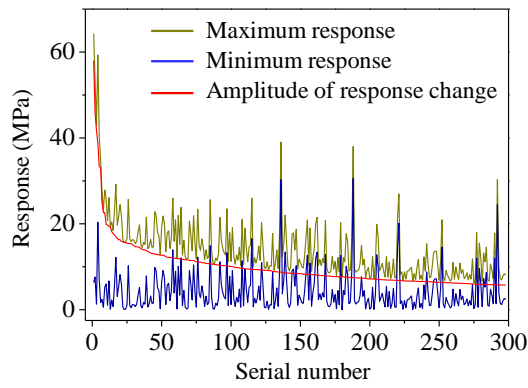


Fig. 10 Changes in σ_{\max}^T and σ_{\min}^T with descending sorting of $\Delta\sigma$

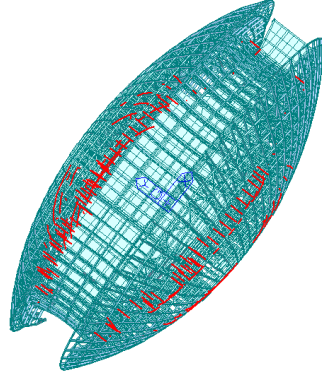


Fig. 11 Overall distribution of 10 sets of bars fluctuating between tension and pressure

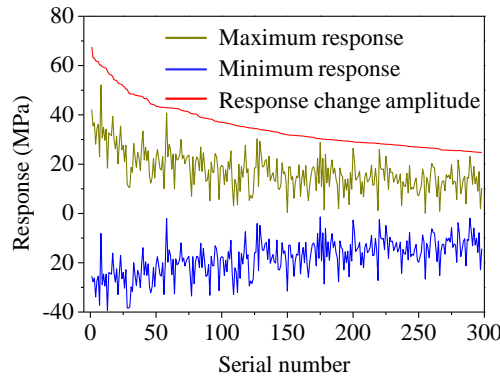


Fig. 12 Changes in σ_{\max}^T and σ_{\min}^P with descending sorting of $\Delta\sigma$

(4) Comparison and analysis of different bar response information types. The first 300 $\Delta\sigma$ bars that were always under pressure were mainly concentrated in the circumferential bar on sides 3 and 4. The first 300 $\Delta\sigma$ bars that were always in tension were mainly concentrated in the longitudinal bar on sides 1 and 2. The first 300 $\Delta\sigma$ bars that fluctuated between tension and pressure were mainly concentrated in the circumferential bar and beam on sides 1, 2, 3 and 4. The proportion of various situations can be seen in Fig. 13, while the value range is displayed in Tables 6 and 7.

The overall response of the bars always in tension is larger than that of the bars always under pressure. The maximum response is 64.3 MPa, which is approximately 18.6% of the steel yield strength $f_y = 345$ MPa. The largest amplitude change is 58 MPa, which is approximately 16.8% of f_y . For the bars fluctuating between tension and pressure, the maximum tensile stress is 52.1 MPa; the maximum compressive stress is 40.9 MPa; the response change amplitudes are larger than those of the bars always in tension or always under pressure; and the maximum value is 61.7 MPa, which is approximately 17.9% of f_y .

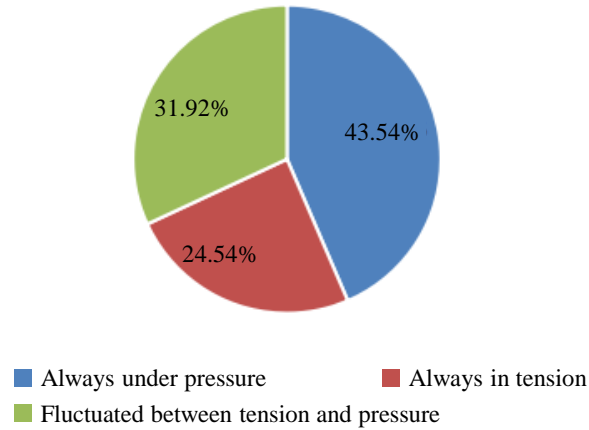


Fig. 13 Proportion of different bar response information types

Table 6 Value range σ_{\max} , σ_{\min} and $\Delta\sigma$ for bars always in tension or under pressure

	σ_{\max} (MPa)	σ_{\min} (MPa)	$\Delta\sigma$ (MPa)
Bars always under pressure	43.7-10.8	30.6-0.5	33.1-8.5
Bras always in tension	64.3-7.0	20.8-1.8	58-5.7

Table 7 Value range σ_{\max}^T , σ_{\max}^P and $\Delta\sigma$ for bars fluctuating between tension and pressure

	σ_{\max}^T (MPa)	σ_{\max}^P (MPa)	$\Delta\sigma$ (MPa)
Bars fluctuating between tension and pressure	52.1-1.3	40.9-1.9	61.7-24.7

7. Conclusions

The temperature and stress data obtained by the sensors were used to analyse the actual temperature effects of the steel space structures. The distribution and scale of the temperature and stress fields were studied. The structure partitions and partition load values were investigated based on the non-uniform distribution characteristics of the thermal effects. The structural temperature partition methods based on solar radiation cumulant were obtained to recognise the overall structural stress field, according to which the members in tension and pressure were sorted to provide an improved understanding of structural behaviour when subjected to the thermal effect.

Acknowledgments

This research is supported by the National Natural Science Foundation of China (Grant Nos. 51678201, 51308162).

References

- Altunok, E., Taha, M.M.R. and Ross, T.J. (2007), "Possibilistic approach for damage detection in structural health monitoring", *J. Struct. Eng.*, **133**(9), 1247-1256.
- Bueno, A. and Sales, S. (2010), "Monitoring of a steel incrementally launched bridge construction with strain and temperature FBGs sensors", *Proceedings of SPIE - The International Society for Optical Engineering*, **7726**, 41-46.
- Cao, Y., Yim, J., Zhao, Y. and Wang, M.L. (2011), "Temperature effects on cable stayed bridge using health monitoring system: A case study", *Struct. Health Monit.*, **10**(5), 523-537.
- Cardini, A.J. and Dewolf, J.T. (2008), "Long-term structural health monitoring of a multi-girder steel composite bridge using strain data", *Struct. Health Monit.*, **8**(1), 47-58.
- Howell, D.A. and Shenton, H.W. (2006), "System for in-service strain monitoring of ordinary bridges", *J. Bridge Eng.*, **11**(6), 673-680.
- Jiang, S. and Hua, X. (2013), "Construction site environment temperature monitoring system based on ZigBee and virtual instrument", *J. Networks*, **8**(4), 963-970.
- Kai, H.H., Halling, M.W. and Barr, P.J. (2006), "Overview of vibrational structural health monitoring with representative case studies", *J. Bridge Eng.*, **11**(6), 707-715.
- Lin, T.Y. and Stotesbury, S.D. (1981), *Structural concepts and systems for architects and engineers*: Wiley.
- Mao, J.X., Wang, H., Feng, D.M., Tao, T.Y. and Zheng, W.Z. (2018), "Investigation of dynamic properties of long-span cable-stayed bridges based on one-year monitoring data under normal operating condition", *Struct. Control Health*.
- Mooney, M.A. (2005), "Vibration-based health monitoring of earth structures", *Struct. Health Monit.*, **4**(2), 137-152.
- Ni, Y.Q., Li, B., Lam, K.H., Zhu, D.P., Wang, Y., Lynch, J.P. and Law, K.H. (2011). "In-construction vibration monitoring of a super-tall structure using a long-range wireless sensing system", *Smart Struct. Syst.*, **7**(2), 83-102.
- Pei, Y., Bai, Y., Shi, Y., Zhu, D. and Wang, Y. (2008), "Temperature distribution in a long-span aircraft hangar", *Tsinghua Sci. Technol.*, **13**(2), 184-190.
- Real, P.M.M.V., Lopes, N., Silva, L.S.D. and Franssen, J.M. (2007), "Parametric analysis of the lateral - torsional buckling resistance of steel beams in case of fire", *Fire Safety J.*, **42**(6-7), 416-424.
- Sohn, H., Czarnecki, J.A. and Farrar, C.R. (2000), "Structural health monitoring using statistical process control", *J. Struct. Eng.*, **126**(11), 1356-1363.
- Teng, J., Lu, W., Wen, R. and Zhang, T. (2015), "Instrumentation on structural health monitoring systems to real world structures", *Smart Struct. Syst.*, **15**(1), 151-167.
- Teng, J., Xiao, Y., Liu, C., Yu, H. and Liu, H. (2012), "Practical structural health monitoring systems in large space structures", *The Workshop on Thirteenth Asce Aerospace Division Conference on Engineering*, 1177-1186.
- Watson, C., Watson, T. and Coleman, R. (2007), "Structural monitoring of cable-stayed bridge: Analysis of GPS versus modeled deflections", *J. Surv. Eng.*, **133**(1), 23-28.
- Yi T.H., Huang H.B. and Li H.N. (2017), "Development of sensor validation methodologies for structural health monitoring: A comprehensive review", *Measurement*, **109**, 200-214.
- Zang, C., Friswell, M.I. and Imregun, M. (2007), "Structural health monitoring and damage assessment using frequency response correlation criteria", *J. Eng. Mech.*, **133**(9), 981-993.
- Zhou, A.T. and Hua, Y. (2008), "Displacement monitoring analysis of a stadium reticulated shell structure during construction process using optical apparatus", *Proceedings of the International Conference on Experimental Mechanics 2008 and Seventh Asian Conference on Experimental Mechanics*, 73750L.

